

# A three-dimensional classification for mathematical pore shape description in complex carbonate reservoir rocks

Steven Claes<sup>1</sup> · Jeroen Soete<sup>1</sup> · Veerle Cnudde<sup>2</sup> · Rudy Swennen<sup>1</sup>

Received: 13 October 2014 / Accepted: 9 April 2016 / Published online: 24 May 2016  
© International Association for Mathematical Geosciences 2016

**Abstract** Porous carbonates display some of the most complex porosity networks in reservoir rocks. This requires a quantitative geometric description of the complex (micro)structure of the rocks. Modern computer tomography techniques permit acquiring detailed information concerning the porosity network in three dimensions. These datasets allow a more objective pore classification based on mathematical parameters. In this study, ratios of the longest, intermediate, shortest dimensions and compactness of the pore shapes, based on an approximating ellipsoid, are analysed to obtain a thorough and objective description of pore shapes. Using intrinsic properties of the latter, the classification can be used at every resolution scale. Five shape classes are defined: rod, blade, plate, cuboid and cube. An additional advantage of this classification is that the data provide information about the orientation of the pores. This allows assessing the anisotropy of the porosity parameter. Apart from having an objective pore-type classification, analysing the shape and orientation of the pores permits to study the relationship with other important petrophysical rock characteristics such as permeability, acoustic properties and rock mechanical behaviour.

**Keywords** Porosity classification · Computer tomography · Continental carbonates · Hydrothermal dolomite

---

✉ Steven Claes  
steven.claes@ees.kuleuven.be

<sup>1</sup> Department of Earth and Environmental Sciences, KU Leuven, Celestijnenlaan 200 E, 3001 Heverlee, Belgium

<sup>2</sup> Department of Geology and Soil Sciences-UGCT, Ghent University, Krijgslaan 281 S8, 9000 Ghent, Belgium

## 1 Introduction

The most frequently applied porosity classification system in carbonate rocks by petroleum geologists is the classification introduced by [Choquette and Pray \(1970\)](#) or is based on it. This classification mainly relates to the sedimentological characteristics of the samples and hence is closely linked to the depositional environment, diagenetic history, fracturing and origin of the carbonates studied. This classification is still widely in use and is cited as the principal system for the classification of porosity in carbonates in various reference books such as [Tucker and Wright \(1990\)](#), [Moore \(2002\)](#), [Keary \(2001\)](#), [Scholle and Ulmer-Scholle \(2003\)](#), [Pentecost \(2005\)](#) and [Ahr \(2011\)](#). More petrophysically based porosity classifications were developed by [Archie \(1952\)](#) and [Lucia \(1995\)](#). These classifications aim to establish a link between porosity types and fluid flow properties. However, the disadvantage of all these classifications is the subjectivity of describing the abundance and shape of the pores and hence not making a correct and objective interpretation of the porosity parameter. More recently [Lønøy \(2006\)](#) introduced a useful classification based on pore characteristics and sizes. The latter author is also one of the first to add a measure addressing the porosity distribution in his classification, and divide samples between uniform and patchy distribution of the pores. However, all the proposed parameters are still mostly descriptive and relative to each other. The rock is described by information about the porosity type, rather than definition of the pore geometry (e.g., intercrystal or interparticle porosity). Hence, the problem remains of correctly assessing the porosity distribution based on parameters deduced from a two-dimensional (thin)-section of the sample. To acquire sufficient and correct information about the porosity distributions, the step towards three-dimensional datasets needs to be made. To link it with permeability values and other rock parameters such as acoustics measurements and dynamic shear moduli, an understanding of the pore geometry and connectivity in 3 dimensions is essential ([Verwer et al. 2010](#)). This data acquisition can be done using X-ray computed tomography (CT) ([Cnudde and Boone 2013](#)).

The aim of this article is to propose a new, objective and quantitative approach with regard to porosity classification, which is based on the three-dimensional pore shape characteristics and its distribution as acquired by X-ray CT. Despite the fact that shape is one of the most fundamental properties of an object, it remains very difficult to characterise and quantify it objectively. [Blott and Pye \(2008\)](#) provide an excellent overview of shape descriptors, proposed for the description of pebbles by different scientists since 1922. The large number of parameters enumerated by these authors proves the complexity of describing shapes.

In this study, continental carbonates and dolomite rock samples were selected because of their complexity and economic importance. The significance of continental carbonates is proven by the discovery of supergiant fields in the Middle East ([Nurmi and Standen 1997](#)) and, more recently, in the South Atlantic ([Sant'Anna 2004](#); [Wright and Barnett 2015](#)). Continental carbonates used in this study are characterised by a monomineralic framework and large, complex pores, which have characteristic shapes. With regard to dolomites, [Warren \(2000\)](#) stated that dolomite reservoirs host 50 % of the world's hydrocarbon reserves. The latter likely needs to be modified since the discovery of the Pre-Salt oil system. The complexity of carbonate reservoirs orig-

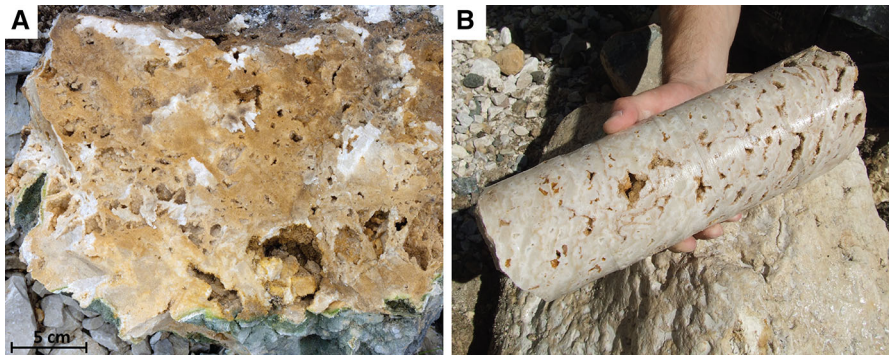


**Fig. 1** Examples of hydrothermal dolomite samples with vuggy porosity: patchy distribution of the vugs (a); uniform, aligned distribution of the vugs (b) according to the classification of (Lønøy 2006)

inates from its various geneses (clastic, biological or chemical) and the susceptibility of carbonates to diagenetic modifications (dissolution, recrystallization and cementation) affecting its reservoir properties. In addition, due to the complex interaction of different precipitation mechanisms, such as physico-chemical, biological and hydrological processes during the formation of continental carbonate deposits one of the most complex and heterogeneous porosity networks is created, especially when the shape of the pores is considered (Pentecost 2005). Moreover, the study of the acoustic response of continental carbonates shows that they follow a different behaviour than marine carbonates (Soete et al. 2015). The difference in pore network architecture plays a major role in explaining the latter difference.

## 2 Materials

Hydrothermal dolomite (HTD) samples are chosen as an example of typical reservoir rocks to test the proposed classification. Porosity in the analysed samples can be subdivided in intercrystalline, moldic and vuggy porosity according to the classification of Choquette and Pray (1970). Intercrystalline porosity mainly corresponds to the voids between matrix dolomite crystals. Pore size varies on average between 20  $\mu\text{m}$  and 500  $\mu\text{m}$ . However, individual moldic pores are on average 3 mm wide and up to 2 cm long. Based on two-dimensional pictures it is hard to determine if these molds are connected. The dominant pore type, on a cm–mm scale, in HTD dolomite is vuggy porosity. The shape of vuggy pores is often complex hence preventing determination of its exact origin. Vug sizes vary between 2 mm and 20 cm (Fig. 1).

Continental carbonate samples used in this study are derived from a study of a kilometre scale natural reservoir analogue system from the Denizli Basin (Turkey) (Claes et al. 2015). As stated in the introduction, porosity networks in the past are mainly described based on two-dimensional classifications proposed by Choquette and Pray (1970), Lucia (2007) and Lønøy (2006). The porosity classification scheme proposed by Choquette and Pray (1970) is based on a differentiation between fabric selective and non-fabric selective porosity types. Most porosity types in continental

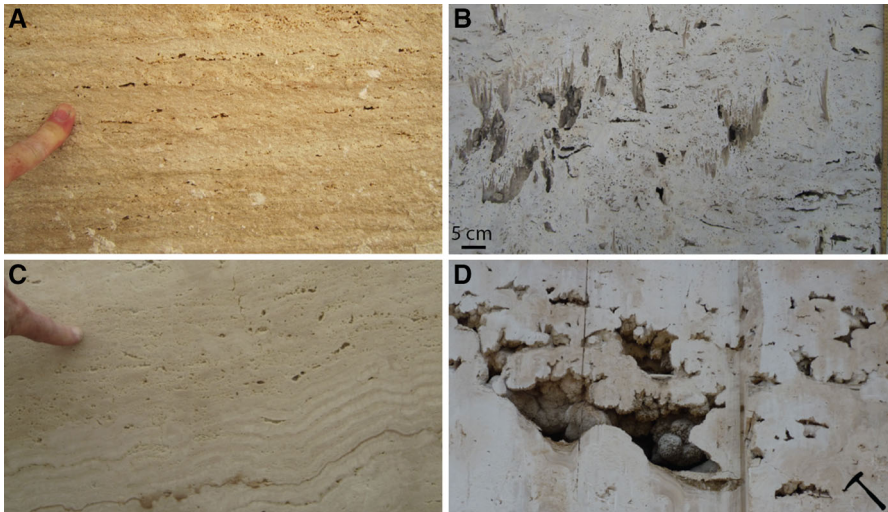


**Fig. 2** Continental carbonate samples: sub-aqueous continental carbonate with porosity aligning on *horizontal layers* (a); sub-areal continental carbonate with moldic porosity originating from plant material (b); sub-aerial continental carbonate showing increased inclination of the layering (c); sub-aerial continental carbonate with shelter like porosity (hammer for scale) (d)

carbonate rocks, visible at micrometre to decimetre scale can be subdivided in the fabric selective category according to Choquette and Pray (1970). Intercrystalline, moldic, fenestral and shelter porosity are the most common porosity sub-types in continental carbonates (Pentecost 2005). On a larger, metre scale, non-fabric selective porosity occurs as fracturing and cavernous porosity created by shelter or secondary porosity.

In this study, continental carbonate samples belong either to those that were deposited sub-aqueously and those that reflect sub-aerial depositional conditions. The porosity in sub-aqueous continental carbonate facies is mainly reflected by its sediment parallel lamination. The lamination in the studied material does not exceed a dip angle of  $5^\circ$ . Macroscopically, the longest size of the pores varies between a few mm and 2 cm. The distribution of the pores is accentuated by the sedimentary lamination (Fig. 2a). Using the classification of Choquette and Pray (1970), porosity in these samples can be described as intercrystalline and fenestral. This corresponds to patchy macropores according to Lønøy (2006). Based on thin section observations, the macropores show little connection, except through intercrystalline porosity. Hence, according to Lucia (1995), their porosity is classified as separate vugs. The sub-areal facies are characterised by alternating laminae and beds of dendritic crusts and granular macro-fabrics. The latter are composed of spherules and encrusted plant fragments (Fig. 2b). The porosity types of this depositional setting can be described as moldic, shelter and growth and framework porosity using the system of Choquette and Pray (1970). More porous layers are characterised by molds of macrophytes, which also allow shelter porosity to develop. Hence, a strong correlation exists between plant fragments and moldic porosity. Macrophytes often develop into mound structures. The layering of

these deposits becomes much more inclined (Fig. 2c). The presence of bryophytes results in growth framework porosity. Hence, a strong correlation exists between former plant fragments and moldic porosity (Fig. 2d). Based on the classification of Lønøy (2006) all the pores fall into the moldic or vuggy macro-pore category.

## 3 Methods

### 3.1 Image analysis and pore shapes

X-ray CT is a three-dimensional imaging technique used in different research fields, which allows to obtain information on the internal structure of the investigated object in a non-destructive way (Kak and Slaney 1989). In this study, 20 cores with a diameter of 10 cm were scanned using a Siemens Somatom scanner at a resolution of 0.3 by 0.3 by 0.5 mm voxel size. Notice that the research philosophy outlined below is also applicable on a smaller spatial scale. Instead of using a medical CT scanner, a micro-CT scanner can be used resulting in resolutions in the order of  $(1 \mu\text{m})^3$  and below, depending on the size of the sample (typically 1 mm diameter or less).

To differentiate pores from matrix, an image segmentation needs to be performed. The purpose of this operation is to separate solid phases such as monomineralic rock constituents and air corresponding to pores. Quantitative analysis of the porosity requires a voxel by voxel determination of void and rock phases. In addition common segmentation algorithms such as simple thresholding, edge detecting and active contours need to be mentioned. Wirjadi (2007) provides an exhaustive survey of existing methods. For segmentation an in-house dual-thresholding algorithm is used, based on the principle first described by Canny (1986) for an edge detecting algorithm. The applied dual or hysteresis thresholding uses two intervals of the histogram to determine the segmentation. Voxels corresponding to the first ‘strong’ threshold are classified as foreground voxels, while voxels selected by the second threshold are only considered foreground if they are connected to voxels already selected by the ‘strong’ threshold. The advantages of this algorithm are the reduced sensitivity to residual noise in the dataset and the selection of less insulated foreground voxels.

As the shape of the identified pores will be calculated based on the generated binary images, the segmentation process in any three-dimensional image analysis is very important. Hence, special attention is paid to this segmentation step by comparing the porosity value obtained from the dataset with He porosity measurements for a limited number of 10 cm diameter cores using medical CT technology. To obtain a sufficient number of data points, results of 3.8 cm diameter plugs are added to the dataset, which are scanned by a General Electric Nanotom micro-CT (with a  $15.8 \mu\text{m}^3$  voxel size resolution). Figure 3 displays the correlation between both datasets. The  $r^2$  value of the regression curve is 0.91 which points to a good correlation between porosity values obtained by both approaches. The fitted curve does not pass through zero as it theoretically should. This can be explained by the existence of micro-porosity, which is not detectable due to the resolution of the medical CT scans. This intercept provides an indication of the amount of micro-porosity missed due to the resolution of the medical CT scans.

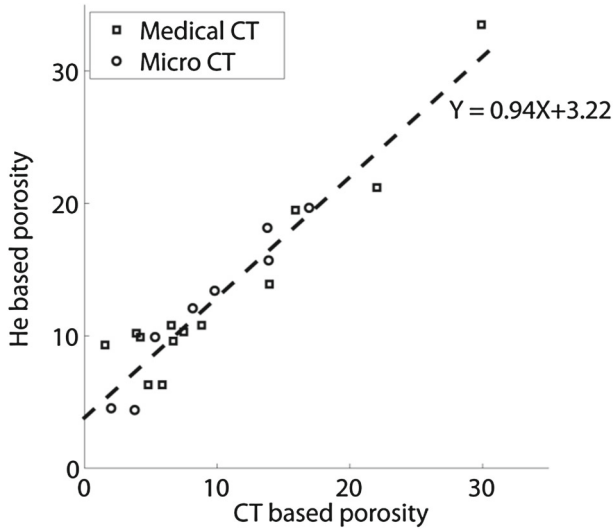


**Fig. 3** Correspondence between He porosity measurements and CT-based porosity measurements

Binarisation of the images, identifying voxels as foreground and background in a two component system like the one with continental carbonates or dolomite versus porosity, is the first step of pore space characterization. From this dataset global quantities such as the total porosity can directly be calculated as well as the volume of interconnected pores. However, additional analysis is essential to understand the petrophysical characteristics of the rocks.

To achieve a correct assessment of the pore shapes it is necessary to split complex pores into elementary pore bodies by determining the pore throats in the three-dimensional dataset. Pore throats are those areas where the pore diameter reaches a local minimum. The identification of these pore throats is performed using a so-called ‘watershed transformation’ approach. The watershed algorithm has many applications in image processing by simulating the flooding from a set of labelled regions in the three-dimensional image. These regions are expanded according to the distance map, until the watershed lines are reached. Hence, the process can be seen as a progressive immersion of a landscape. Three steps are characteristic for this algorithm: (i) calculating the distance map of the binary images, (ii) determining the local maxima in this new dataset, (iii) calculating the dividing lines (watershed lines) between different pore bodies (defined by the local maxima) based on a 26-connectivity in 3 dimensions (Meyer 1994). The process is illustrated on a simple shape in Fig. 4a, where two simple pore bodies connected by a central cuboid are separated. Figure 4b shows the distance map calculated in 3 dimensions and Fig. 4c shows the selected local maxima which are used as centre of the basins in the watershed approach. In Fig. 4d the two pore bodies are separated.

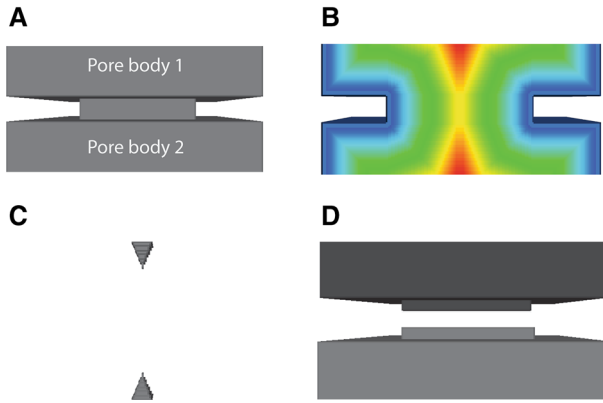


**Fig. 4** Overview of the watershed algorithm: **a** original complex pore; **b** slice of the three-dimensional distance map; *red color* indicates the largest distance from the edge; **c** centre of the basins; **d** resulting pore bodies

### 3.2 Shape parameters

Once the pore space is transferred into three-dimensional images labelled for individual pore bodies and disconnected from each other by rock or through the watershed procedure, the shape parameters of individual pores can be calculated. The focus in characterising pore networks should, in contrast to the Choquette and Pray (1970) classification, shift from rock textures and genesis to the pore geometry. Lønøy (2006) elaborated the classification adding pore size and distribution.

In the proposed classification individual pores are considered as discrete objects, making it possible to calculate the mechanical moments of these objects. The resulting tensor is defined as

$$\begin{bmatrix} I_{xx} & I_{xy} & I_{xz} \\ I_{yx} & I_{yy} & I_{yz} \\ I_{zx} & I_{zy} & I_{zz} \end{bmatrix}.$$

These results are used to calculate several shape parameters and it allows to propose a new, objective and quantitative pore classification system, though using a terminology inspired by the two-dimensional particle classification systems of Blott and Pye (2008).

The spectral theorem for real, symmetric matrices defines that a Cartesian coordinate system exists for which the tensor becomes diagonal having the following form

$$\begin{bmatrix} I_1 & 0 & 0 \\ 0 & I_2 & 0 \\ 0 & 0 & I_3 \end{bmatrix},$$

$I_1$ ,  $I_2$  and  $I_3$  are called the principal moments of inertia. The axes corresponding to this tensor are the principal axis. The tensor and principal axis can be calculated solving the eigenvalue problem of the original tensor.

Using the principal moments of inertia it becomes possible to calculate the three principal dimensions of the approximate ellipsoid based on the known inertia tensor of an ellipsoid. In this tensor the symbols  $L$ ,  $I$  and  $S$  correspond to the longest dimension, the longest dimension perpendicular to  $L$  and the longest dimension perpendicular to  $L$  and  $I$ , respectively

$$\begin{bmatrix} \frac{1}{5}m(I^2 + S^2) & 0 & 0 \\ 0 & \frac{1}{5}m(L^2 + S^2) & 0 \\ 0 & 0 & \frac{1}{5}m(L^2 + I^2) \end{bmatrix}.$$

Parameters  $V_s$  and  $E_s$  are used to evaluate the goodness of fit between the pore shape and the approximating ellipsoid. The goodness of fit increases with ratio's approaching 1

$$V_s = \frac{v_{\text{approximating ellipsoid}}}{\text{Volume}},$$

$$E_s = \frac{e_{\text{approximating ellipsoid}}}{\text{Surface}}.$$

Because a labelled dataset, based on connectivity, is used for calculating  $L$ ,  $I$  and  $S$ , complex parts of the porosity network show  $V_s$  and  $E_s$  ratios diverting from 1. To solve this problem, these pores are divided into multiple pores by applying the watershed approach again, for which  $L$ ,  $I$  and  $S$  dimensions are calculated again on an individual basis. Notice that the position of the pores can be visualised for inspection.

### 3.2.1 Pore types and classification

The proposed universal porosity classification is based on the actual three-dimensional shape of the pores in terms of the ratio's  $I/L$  and  $S/I$  (Blott and Pye 2008). The advantage in this approach is that it is a simple classification, without calculating derivative parameters. In this classification individual pores are described based on their elongation and flatness, which thus also allows anisotropy of the pore fabric to be assessed. Figure 5 shows a diagram with five defined shape classes, namely rod, blade, cuboid, plate and cubic shapes. This simplified scheme allows objective and automatic description of pores.

### 3.3 Compactness

A parameter that combines information about the surface area and volume of the described shape is the compactness Gonzalez (1987) and Haralick and Shapiro (1991). This parameter is defined as the following ratio  $(\text{volume}^2)/(\text{area}^3)$ , which is dimensionless. Among all three-dimensional shapes with the same volume, the sphere will have a minimum surface area, resulting in a compactness of 1. The compactness is an intrinsic characteristic of the shape and hence is invariant under geometric transformations such as translation, rotation and scaling.



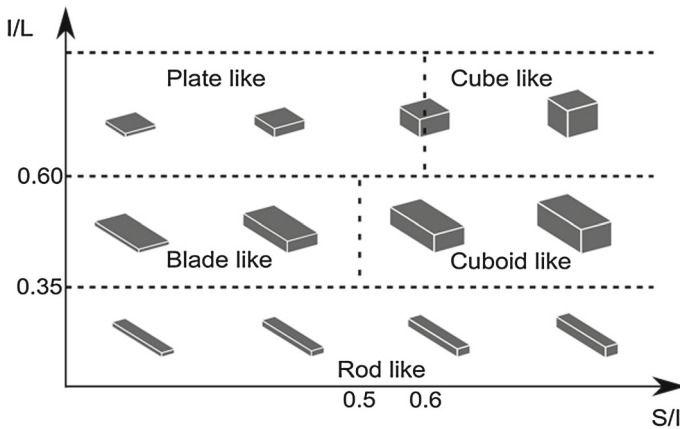


**Fig. 5** Overview of the proposed pore shapes using the ratios of the longest (*L*), intermediate (*I*) and shortest (*S*) pore dimension, based on a projected ellipsoid within the assigned pore

The compactness provides information about the complexity of the shape. A sphere like shape has a compactness value of 1, while a star like shape has a much lower compactness value. Hence, some bias towards the previous defined classes exists. The cube-like shapes will all have a compactness value close to 1, while the plate and rod-like shape classes have the lowest compactness value. However, enough additional information is provided by this parameter, because it provides additional insight in the shape of the pores and its connectivity.

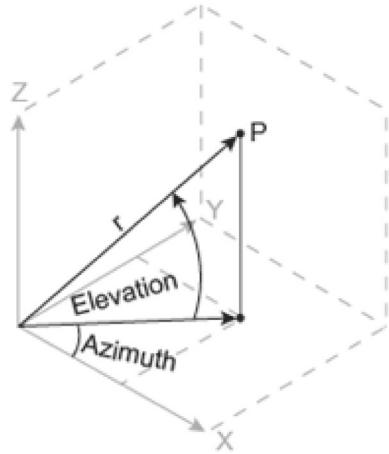
### 3.4 Orientation of the pores

The analysis and interpretation of directional data require specific representations and descriptors. This allows preferential pore orientations and pore space anisotropy to be described. The eigenvectors of the previous described system provide the orientation of the principal directions of the approximating ellipsoid. The orientations are represented in a spherical coordination system as shown in Fig. 6. The azimuth varies between  $-\pi$  and  $\pi$  and the elevation between  $-\pi/2$  and  $\pi/2$ . The directional data are analysed by means of unit length vectors, by representing the angular observations as points on a unit sphere.

However, the mean direction of a set of points on a sphere cannot correctly be calculated by taking the average of the azimuth and elevation values, because the coordinate system used is discontinuous. For example, the average of (0,0) and (359,0) would give the incorrect value of (179.5,0). The correct mean direction of a set of *n* data points ( $P_i = (\theta_i, \varphi_i)$ ) is therefore calculated using the Cartesian coordinates ( $x_i, y_i, z_i$ ) of each point,

$$\begin{aligned}
 x_i &= \sin \theta_i \cos \varphi_i \\
 y_i &= \sin \theta_i \sin \varphi_i \\
 z_i &= \cos \theta_i
 \end{aligned}$$

**Fig. 6** Illustration of the coordinate system, defining azimuth and elevation. Arrows indicate positive directions



$$R = \left( \sum_{i=1}^n x_i \quad \sum_{i=1}^n y_i \quad \sum_{i=1}^n z_i \right).$$

The mean direction of the  $n$  points can be obtained using the above formula, yielding a resultant length of the mean direction. The value of  $R$  varies between 0 and  $n$ , because of the use of unit vectors. A high value corresponds to a low dispersion of the data points, while low values are typical for uniformly distributed data points (Wightman and Kistler 1989). The normalised version of this parameter is indicated with  $R_n$  and varies between 0 and 1. Hence, the mean directions can be calculated using the direction cosines, which can be reconverted to spherical coordinates

$$\theta = \arccos(\bar{z}) \quad \phi = \arctan \left( \frac{\bar{y}}{\bar{x}} \right).$$

## 4 Results

### 4.1 Dolomite versus continental carbonate

The proposed classification provides an objective approach to compare the porosity network of dolomite and continental carbonate samples. The question indeed arises whether the pore characteristics are different seen the dominance in both lithologies of moldic and vuggy pores. Table 1 provides an overview of the poreshape distribution in 10 samples for both lithologies.

A method for comparing the means of the different shapes of both lithologies is one-way ANOVA (analysis of variance) analysis. The null hypothesis of this statistical test is

$$H_0 : \mu_1 = \mu_2 = \dots = \mu_n.$$

**Table 1** Overview of the pore shape distribution based on percentages in continental carbonate and dolomite samples

	Porosity	Rod	Blade	Cuboid	Plate	Cube
Dolo 1	4.8	0.08	0.11	0.34	0.25	0.23
Dolo 2	5.0	0.08	0.09	0.39	0.22	0.22
Dolo 3	6.3	0.08	0.10	0.35	0.25	0.22
Dolo 4	6.4	0.11	0.15	0.29	0.24	0.21
Dolo 5	6.8	0.09	0.10	0.31	0.22	0.29
Dolo 6	7.2	0.08	0.11	0.33	0.25	0.24
Dolo 7	7.6	0.10	0.13	0.30	0.24	0.22
Dolo 8	8.2	0.09	0.10	0.35	0.22	0.24
Dolo 9	8.2	0.07	0.09	0.35	0.21	0.28
Dolo 10	8.5	0.10	0.09	0.36	0.20	0.25
C.C. 1	3.2	0.10	0.13	0.33	0.21	0.24
C.C. 2	4.2	0.07	0.07	0.36	0.17	0.32
C.C. 3	5.4	0.12	0.10	0.33	0.21	0.24
C.C. 4	6.9	0.16	0.12	0.30	0.21	0.21
C.C. 5	7.2	0.20	0.12	0.30	0.19	0.19
C.C. 6	8.6	0.17	0.12	0.29	0.20	0.22
C.C. 7	9.1	0.17	0.11	0.31	0.20	0.21
C.C. 8	9.6	0.14	0.12	0.31	0.21	0.23
C.C. 9	11.6	0.26	0.10	0.30	0.16	0.19
C.C. 10	13.1	0.17	0.11	0.31	0.22	0.19

Rejecting this null hypothesis means that both groups are different and hence a distinction can be made based on the studied pore shape. The test is rejected if the resulting  $P$  value is lower than 0.05. Figure 7 provides an overview of the  $P$  values for each defined pore shape. Three out of 5 pore shape classes are significantly different when comparing dolomite and continental carbonate samples. The largest difference can be found in the rod and blade-like shaped pores. This is also shown in Fig. 7f with all the boxplots compared for the different shapes.

#### 4.2 Sub-aqueous versus sub-aerial continental carbonates

With regard to the studied continental carbonate samples a genetic differentiation between sub-aqueous and sub-aerial facies types can be made. The question arises whether the apparent difference in characteristics of the porosity network between both facies types can be quantified. Figure 8 illustrates some representative three-dimensional reconstruction of both porosity network characteristics.

Table 2 and Fig. 9 give the pore shape distribution for seven sub-aqueous and eight sub-aerial samples. The ANOVA analysis shows that a distinction can be made based on rod and blade-shaped pores. The plate-like shaped pores are not significantly

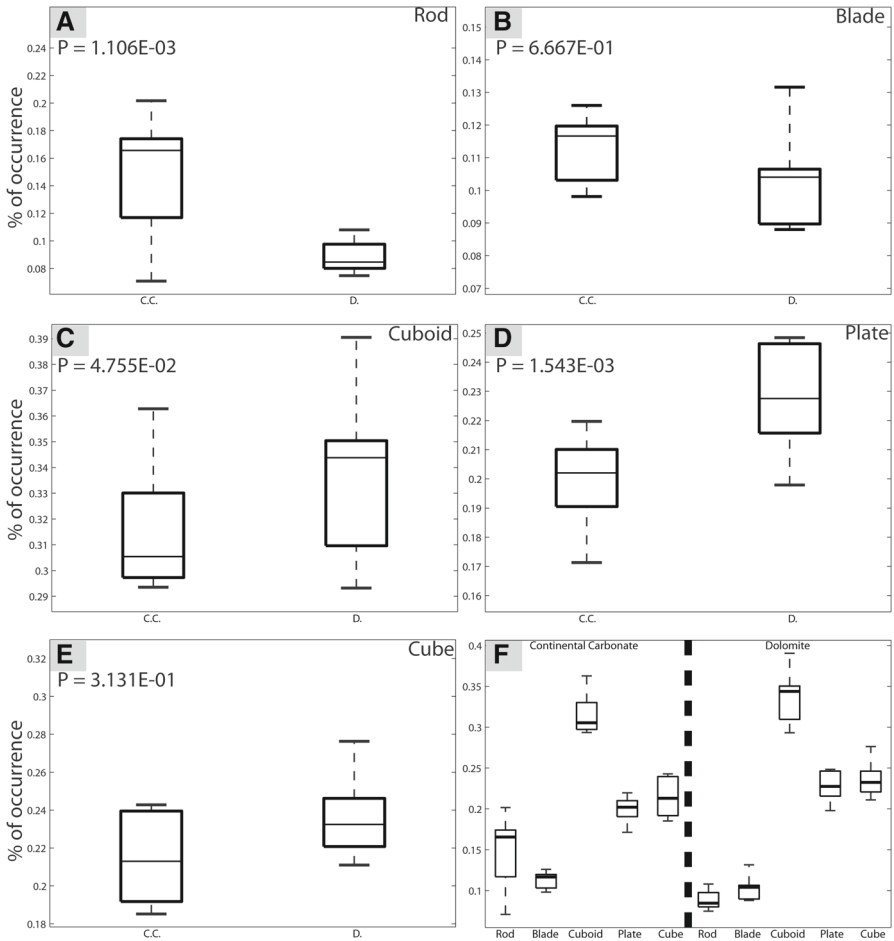


**Fig. 7** Boxplots of the shape distribution in dolomite (D.) and continental carbonate (C.C.) samples: **a** rod-like shape; **b** blade-like shape; **c** cuboid-like shape; **d** plate-like shape; **e** cube-like shape; **f** comparison of the occurrence percentage of pore shapes in continental carbonates and dolomite samples

different; however, if the volume distribution of the pores are taken into account, the difference becomes significant ( $P = 0.023$ ).

### 4.3 Compactness and clustering

As a third parameter, compactness can be taken into account to develop a more thorough description of the pore body shape. Different data points of individual pore body characteristics of one core are plotted and clustered by the  $k$ -means algorithm in Fig. 10 (Seber 1984). This algorithm partitions the points into 5 clusters based on an iterative way of minimising the sum, over all clusters, of the within-cluster sums of point-to-cluster-centroid distances. This objective distribution shows similarities with

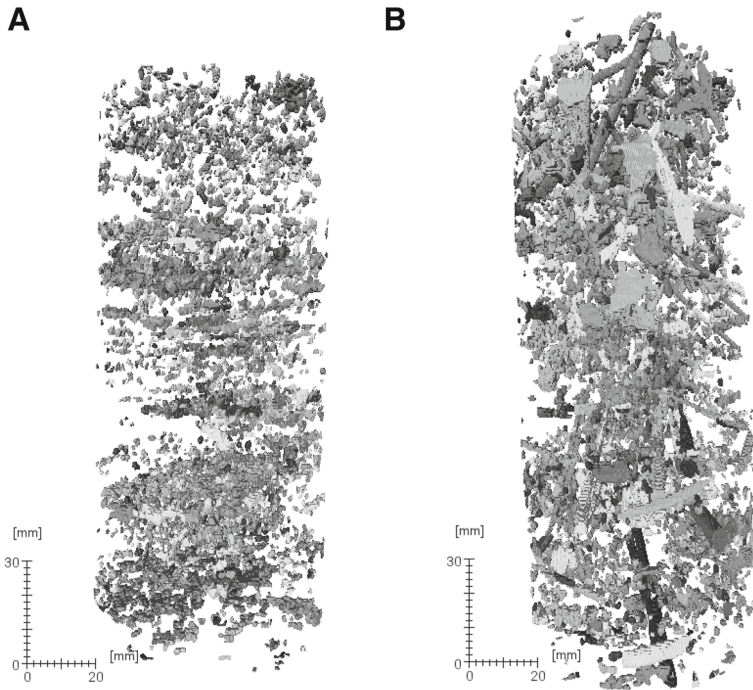


**Fig. 8** Three-dimensional volume rendering of the porosity network in continental carbonates: **a** sub-aqueous sample; **b** sub-aerial sample

**Table 2** Overview of the pore shape distribution in sub-aqueous and sub-aerial continental carbonate samples

	Porosity	Rod	Blade	Cuboid	Plate	Cube
Sub-aqueous	3.2	0.10	0.13	0.33	0.21	0.24
Sub-aqueous	3.9	0.06	0.08	0.30	0.16	0.40
Sub-aqueous	4.2	0.07	0.07	0.36	0.17	0.32
Sub-aqueous	4.2	0.09	0.08	0.29	0.20	0.33
Sub-aqueous	5.4	0.12	0.10	0.33	0.21	0.24
Sub-aqueous	6.5	0.08	0.09	0.32	0.20	0.32
Sub-aqueous	7.5	0.11	0.09	0.29	0.18	0.33
Sub-aerial	7.9	0.14	0.10	0.32	0.19	0.26
Sub-aerial	6.9	0.16	0.12	0.30	0.21	0.21
Sub-aerial	8.6	0.20	0.12	0.30	0.19	0.19
Sub-aerial	8.6	0.17	0.12	0.29	0.20	0.22
Sub-aerial	9.1	0.17	0.11	0.31	0.20	0.21
Sub-aerial	9.6	0.14	0.12	0.31	0.21	0.23
Sub-aerial	11.6	0.26	0.10	0.30	0.16	0.19
Sub-aerial	13.1	0.17	0.11	0.31	0.22	0.19

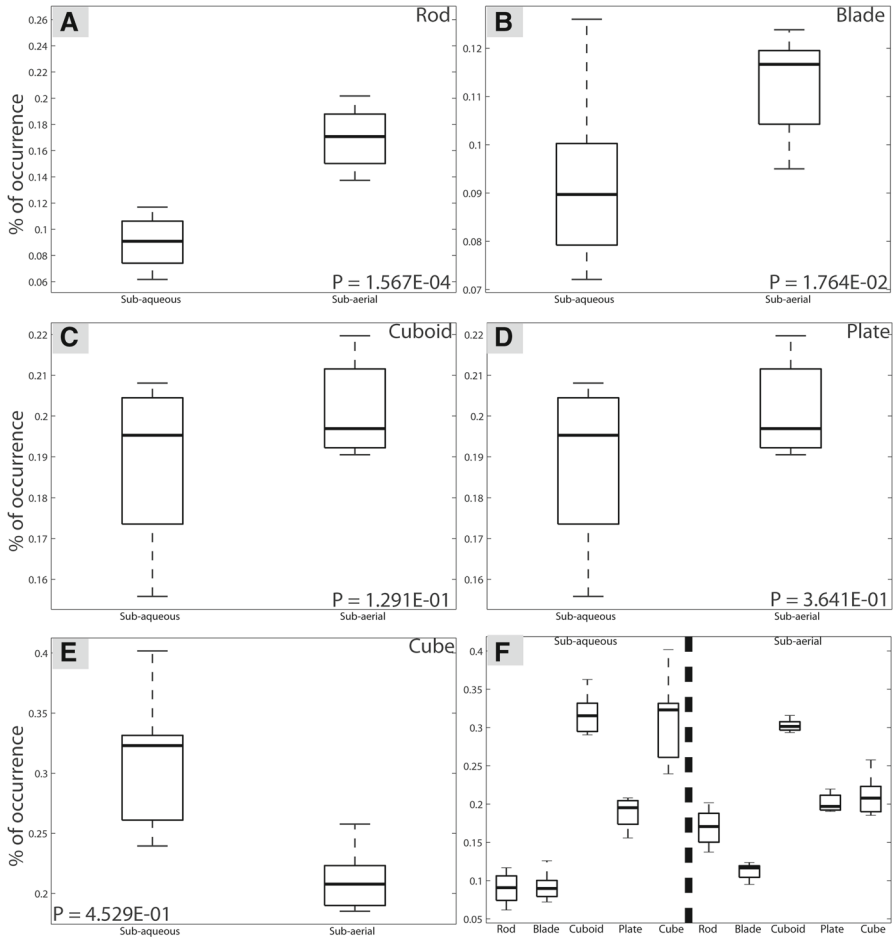


**Fig. 9** *Boxplots* of the shape distribution in sub-aqueous and sub-aerial continental carbonate samples: **a** rod-like shape; **b** blade-like shape; **c** cuboid-like shape; **d** plate-like shape; **e** cube-like shape; **f** comparison of % of occurrence of sub-aqueous and sub-aerial continental carbonate samples

the earlier proposed pore classification. Cluster 5 corresponds to the cube-like shape pore bodies. Cluster 1 and 3 matches the cuboid and blade-like shape pores, respectively. The final two clusters (2 and 4) can, respectively, be associated with the plate and rod-like shaped pore bodies. It should be noted that boundaries are transitional.

#### 4.4 Pore orientation

The advantage of the previous classification is that it provides an objective and fast way to select the different pore shapes present in the examined sample and allows to examine the contribution of each pore shape to the entire porosity network. Moreover, the three-dimensional dataset allows to view the spatial distribution of the pores as

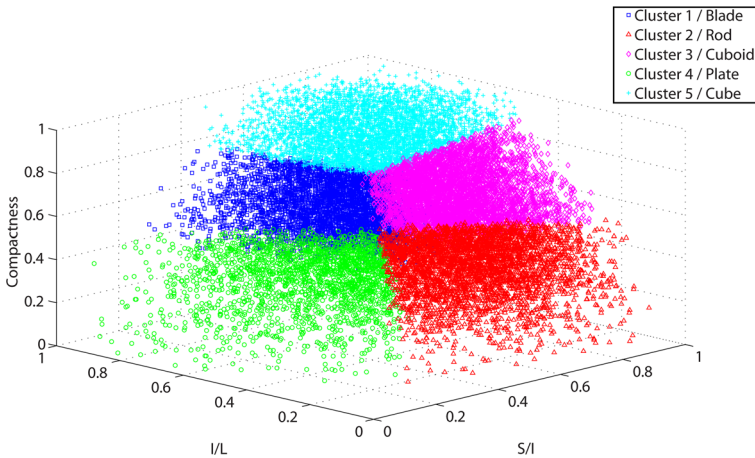


**Fig. 10** Result of the  $k$ -means clustering of a continental carbonate core based on the ratios of the longest ( $L$ ), intermediate ( $I$ ), shortest ( $S$ ) pore dimension and the compactness parameter

well as to analyse the orientation of individual pore bodies. The orientation of the longest dimensions of the pores provides insight with respect to the anisotropy concerning porosity in the studied samples. The orientation of pore shapes such as rod and plate-like shapes can provide important information, to understand the petrophysical properties of samples, especially the permeability of the sample for which the direction of the measurement is important. Hence, elongated shapes play an important role in connecting different porous zones in the samples. Based on the previous defined classification, especially the rod and plate shaped pores have the potential to connect different pore clusters.

In Fig. 11 rod shaped pores of two different continental carbonate samples are selected. On the left-hand side of each figure a spherical plot, showing the projection of the unit sphere with markers for the points corresponding to the longest direction of each pore is given. In Fig. 11a most rod-like shaped pores are aligned in a vertical orientation, resulting in an  $R_n$  value of 0.80. The standard deviation corresponds to an angle of  $38^\circ$ . In the example shown in Fig. 11b the orientation of the rod-like shapes is much more uniformly distributed. For this example the  $R_n$  parameter is equal to 0.28 and has a much larger standard angle of  $91^\circ$ . Hence, a  $R_n$  value approaching 1 and a small standard deviation angle indicate a good alignment of the selected pores. Moreover, for these samples, it allows to draw conclusions about the growth direction of the plant fragments and establish if they are still in their growth position as is the case in Fig. 11a.

As stated above, also the plate shaped pores have the potential to connect different porous zones in the samples. In Fig. 12 the alignment of plate-like shapes in a subaqueous continental carbonate and hydrothermal dolomite are selected. In the former sample the plate-like shapes are clearly aligned in a horizontal direction (Fig. 12a). However, the orientations on the unit sphere are less uniformly distributed ( $R_n = 0.3$ ), but most points are situated around the equator. For the dolomite sample, the points on the unit sphere cluster around two directions (Fig. 12b). This observation is confirmed by a low  $R_n$  value of 0.43. The perpendicularity of both clusters can be explained by

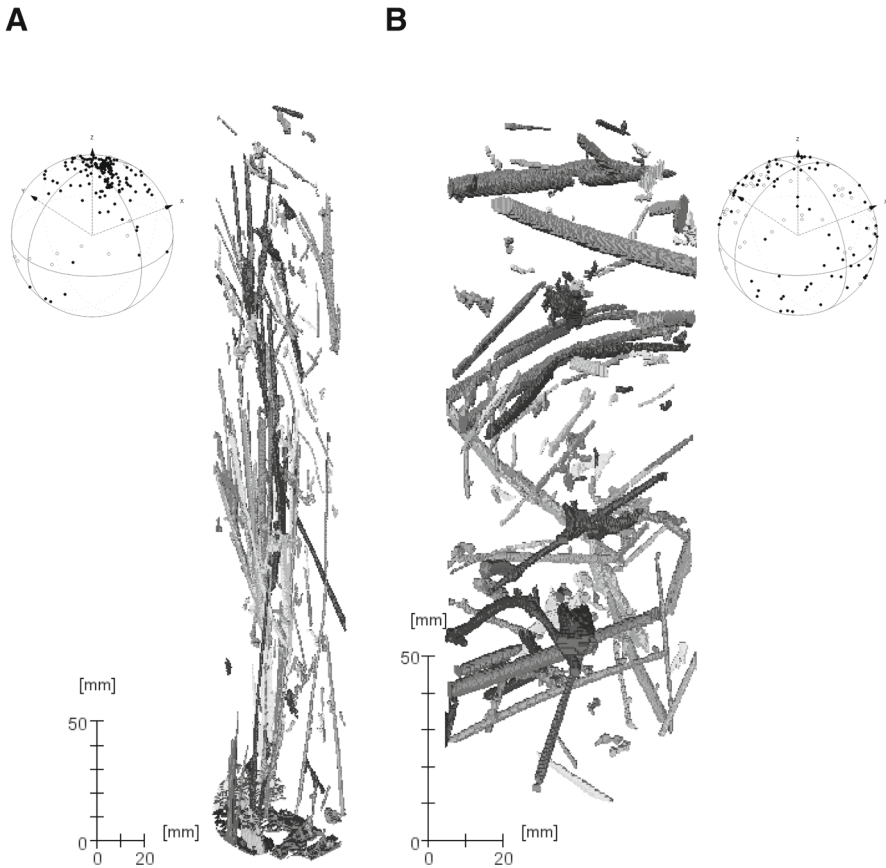


**Fig. 11** **a** Three-dimensional visualisation of the rod-like shaped pores, originating from reed stems, which are aligned in the vertical direction and a representation of the direction of the longest dimension ( $L$ ) (Sphere in left upper corner); **b** three-dimensional visualisation of the rod-like shaped pores, which are randomly aligned and a representation of the direction of the longest dimension ( $L$ ) (Sphere in right upper corner)

the shape of the plates. One group is characterised by an elongated plate-like shape, while the other group is more compact and represents the transition towards a cuboid shaped pore.

## 5 Discussion

This paper documents the implementation of a novel approach towards universal, objective and quantitative porosity and pore shape classification in 3 dimensions using computer tomography. This classification is based on different parameters such as the dimensions of the pores, the compactness and the orientation of the longest dimensions of the approximating ellipsoid. In the past several parameters were defined for different applications resulting in a multitude of descriptors such as the ones defined by [Wentworth \(1923\)](#), [Krumbein \(1941\)](#) and [Dobkins and Folk \(1970\)](#). The use of



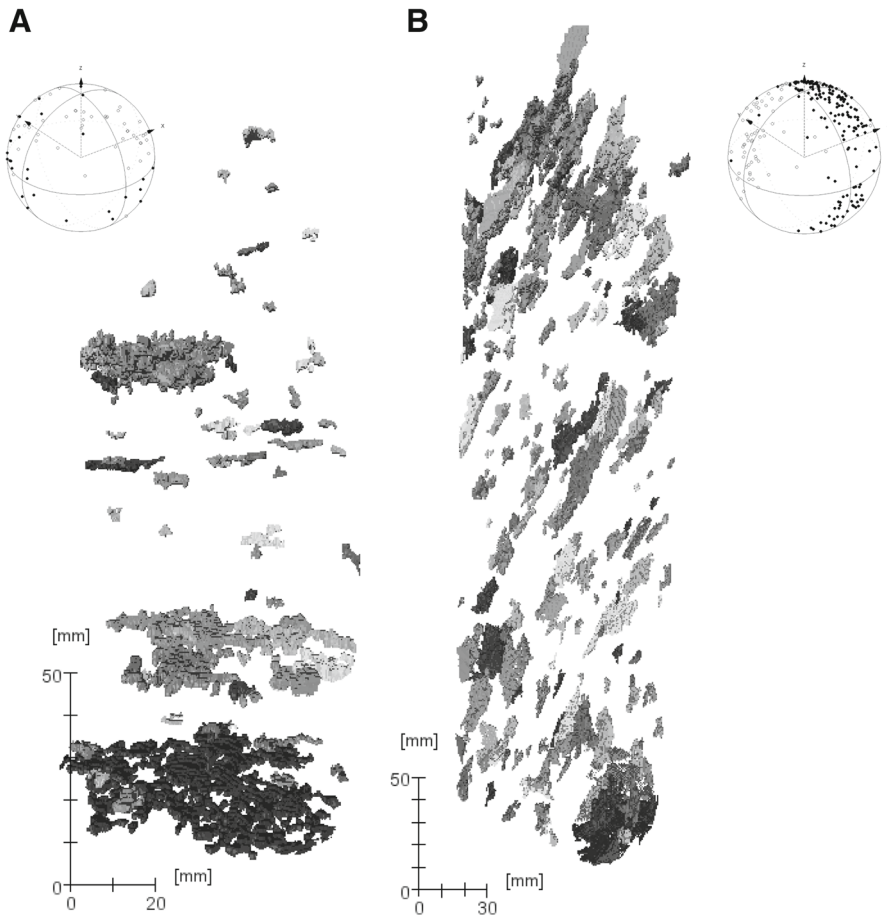


**Fig. 12** Three-dimensional visualisation of selected plate-like shaped pores: **a** in a representative sub-aqueous continental carbonate sample, which are *horizontally aligned* and a representation of the direction of the longest dimension ( $L$ ) (*sphere in left upper corner*); **b** in a representative hydrothermal dolomite sample, where the pores are aligned and a representation of the direction of the longest dimension ( $L$ ) (*sphere in right upper corner*)

general invariant parameters allows to obtain a broad appropriate application range. Moreover, this classification is not scale dependent and is thus applicable for different spatial scales. Micro-CT also provides excellent datasets to be used in the proposed classification.

The results show the clear differences of pore shape parameters in distinct lithologies, such as hydrothermal dolomite and continental carbonate rocks. This conclusion on itself is not new, but the differences between both porosity networks are objectified using mathematical parameters. The pore shape distribution as well as the general orientation of the pores in both lithologies shows a distinctive pore network. In this case the difference between both lithologies can primarily be made based on rod, plate and cuboid shaped pores as indicated by the respective  $P$  values (Fig. 7). The smaller

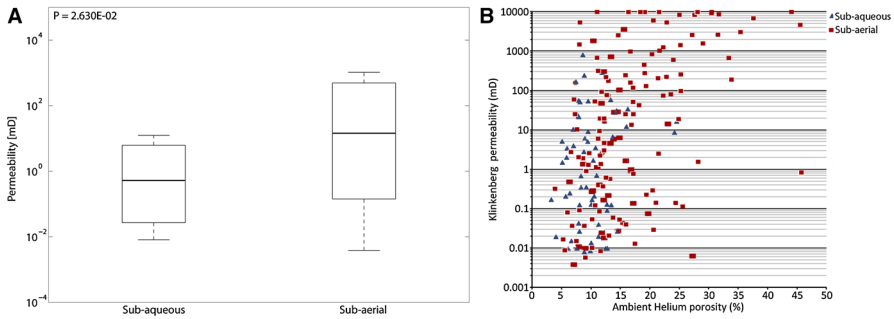


**Fig. 13** **a** Boxplots of the permeability values of sub-aqueous and sub-aerial continental carbonate lithologies; **b** porosity—permeability plot of the data

the  $P$  value the larger the observed difference between both lithologies. This can be explained by the observation that rod pore shapes are more typical for continental carbonate rocks, where they relate to decayed reed stems. The latter are obviously not present in hydrothermal dolomites. Plate and cuboids-like shapes are more abundant in dolomite rock samples, which are characterised by intercrystalline and vuggy porosity and translate into the predominance of the mentioned pore shapes.

In continental carbonate rocks a broader spectrum of pore shapes is more common, resulting in one of the most complex porosity networks observed in reservoir rocks in general. Also, this observation is highly dependent on the facies type of the studied sample as the complexity of the pore network is closely related to the increased biological aspect of continental carbonates. The pore shape distribution allows to differentiate between sub-aqueous and sub-aerial facies types. The distinction between both facies types can be primarily made based on rod, blade and cube-like shapes (Fig. 9). Rod-like shapes are much less common in sub-aqueous facies, while cube-like shapes are more abundant in this facies type. Also the plate-like shapes are more important in volume if they are present. These correspond with connected pores originating from the decay of organic matter, which was encrusted by calcite layers. This observation from the CT analysis matches with macroscopical observations of the sub-aqueous and sub-aerial continental carbonate facies. Using the pore classification proposed by [Choquette and Pray \(1970\)](#) most pores in continental carbonates are described as moldic, shelter and growth framework, while according to [Lucia \(2007\)](#) most of the segmented pores would be classified as vuggy porosity. [Lucia \(2007\)](#) further subdivided the pore space in separated and interconnecting vugs. However, interconnectivity is difficult to assess based on two-dimensional information. Separated vugs are not connected to each other. Hence, they increase the total porosity but not necessarily the permeability. However, intercrystalline porosity may still connect these vugs. If the vugs are interconnecting, the permeability of the sample will be well above the value expected from an interparticle pore system with the same porosity value.

The proposed classification based on CT data provides additional tools for geologists and reservoir engineers to objectify the description of pore networks in reservoir rocks. The classification provides a toolbox to make the description more uniform and solely based on the shape of the pores. Previously proposed classifications require a

two-dimensional interpretation about the shape of the pores as well as the context of the surrounding rock phase (e.g., interparticle versus intraparticle porosity). Hence, in the past the quality of the description depended a lot on the experience of the scientist. Moreover, the advantage of the  $k$ -means clustering approach is the complete objectivity of the method. In a matter of minutes the porosity network of a 10 cm diameter core with a height of 30 cm can be analysed. The duration of the analysis highly depends on the number of pore(-bodies) present in the core. However for the visualisation of the different labelled pore bodies, a high-end computer with sufficient RAM-memory as well as specialised software for three-dimensional rendering is required. These requirements become more important if datasets of a micro-CT are used, because these tend to be double or triple in size.

The distribution and shape of the pores play an important role on interpreting the relationship between porosity and permeability. Three-dimensional information helps to better understand and interpret this relationship. Alignment of pores and preferential fluid pathways not only become visualised and allow a more thorough interpretation but their alignment can be quantified. For example, the more common presence of rod and blade-shaped pores in sub-aerial facies types affects the petrophysical properties. Permeability values of sub-aerial samples are significantly higher than sub-aqueous samples. Rod and blade-shaped pores create long pathways, which can connect permeable zones in the samples. Figure 13 illustrates this feature based on a large dataset ( $n = 200$ ) of 2.5 cm diameter plugs.

Moreover, the orientation of the pores influences the permeability tensor. For example, the sample in Fig. 11b has a vertical permeability of 0.97 mD, while the horizontal permeability varies between 240 and 300 mD. Also in sub-aqueous continental carbonate the permeability tensor is dominated by horizontal plate shaped pores (Fig. 12), resulting in a permeability which is two orders of magnitude larger parallel to these plates when compared to pores aligned in a perpendicular direction.

The shape of the pores also proves to be of importance with regard to the acoustic properties of rock samples (Soete et al. 2015). In the latter study it was shown that rod and cuboid shaped pores increase compressional wave velocities, while flattened pore shapes such as blade and plate-like shaped pores decrease the acoustic wave propagations. These observations help to understand more accurately acoustic properties of reservoir rocks. The cited examples illustrate the broad influence of pore shapes on different reservoir and petrophysical properties, as for example permeability and acoustic impedance. Consequently a comprehensive study of the pore shapes will allow to better understand the correlation of the related parameters and should result in developing more accurate reservoir models.

## 6 Conclusions

In this study, a new porosity classification approach is proposed based on intrinsic three-dimensional shape parameters such as the ratios of the longest, intermediate and shortest pore dimension and the compactness of pore bodies. This classification has the advantage of being objective, quantitative and universal as it can be used at different spatial scales, for example from  $\mu\text{m}$  to m scale. Using this classification, pore

characteristics of different rock lithologies such as dolomite and continental carbonate can be distinguished in a statistically significant way based on a limited number of samples. Moreover, pore features in continental carbonate rock samples can be further differentiated between sub-aqueous and sub-aerial facies types. This approach allows automating and objectifying the process of pore determination in function of facies.

An additional advantage of this classification is the information it provides about the orientation of the pores. Analysing the direction of the longest dimension allows to assess the anisotropy of the porosity parameter and to better assess the relationship with the permeability parameter.

The additional three-dimensional information provided by this new proposed classification helps to better understand the rock and petrophysical properties of reservoir rocks. A correct pore type identification and evaluation has a major influence on reservoir characterisation and hence has important economic implications.

**Acknowledgments** The authors wish to acknowledge the Fund for Scientific Research—Flanders (FWO) for providing a Research Grant to the first author as well as the Hercules foundation (Flanders) for founding the micro- and nano-CT project for the hierarchical analysis of materials as well as the staff of the radiology department of UZ Leuven. Finally we would like to thank the reviewers for their constructive comments.

## References

- Ahr W (2011) *Geology of carbonate reservoirs: the identification, description, and characterization of hydrocarbon reservoirs in carbonate rocks*. Wiley, New York
- Archie GE (1952) Classification of carbonate reservoir rocks and petrophysical considerations. *AAPG Bull* 36(2):278–298
- Blott SJ, Pye K (2008) Particle shape: a review and new methods of characterization and classification. *Sedimentology* 55(1):31–63
- Canny J (1986) A computational approach to edge detection. *IEEE Trans Pattern Anal Mach Intell PAMI* 8(6):679–698
- Choquette P, Pray L (1970) Geologic nomenclature and classification of porosity in sedimentary carbonates. *Am Assoc Pet Geol Bull* 54(2):207–250
- Claes H, Soete J, Van Noten K, El Desouky H, Marques Erthal M, Vanhaecke F, Özkul M, Swennen R (2015) Sedimentology, three-dimensional geobody reconstruction and carbon dioxide origin of Pleistocene travertine deposits in the Ballik area (south-west Turkey). *Sedimentology* 62:1408–1445
- Cnudde V, Boone MN (2013) High-resolution X-ray computed tomography in geosciences: a review of the current technology and applications. *Earth Sci Rev* 123:1–17
- Dobkins JE Jr, Folk RL (1970) Shape development on Tahiti-nui. *J Sediment Petrol* 40(4):1167–1203
- Gonzalez RC (1987) *Digital image processing*. Addison-Wesley Publishing Company, Reading
- Haralick RM, Shapiro LG (1991) Glossary of computer vision terms. *Pattern Recognit* 24 No 1(1):69–93
- Kak AC, Slaney M (1989) *Principles of computerized tomographic imaging*. IEEE Press, New York
- Keary P (2001) *The new Penguin dictionary of geology*. Penguin Books, London
- Krumbein WC (1941) Measurement and geological significance of shape and roundness of sedimentary particles. *J Semmentary Petrol* 11(1):64–72
- Lønøy A (2006) Making sense of carbonate pore systems. *AAPG Bull* 90(9):1381–1405
- Lucia FJ (2007) *Carbonate reservoir characterization: an integrated approach*. Springer Science & Business Media, New York
- Lucia FJ (1995) Rock-fabric/petrophysical classification of carbonate pore space for reservoir characterization 1. *AAPG Bull* 9(9):1275–1300
- Meyer F (1994) Topographic distance and watershed lines. *Signal Process* 38(1):113–125
- Moore CH (2002) *Carbonate reservoirs porosity evolution and diagenesis in a sequence stratigraphic framework*. Elsevier, Amsterdam
- Nurmi R, Standen E (1997) Carbonates: the inside story. *Middle East Well Eval Rev* 18:28–41

- Pentecost A (2005) *Travertine*. Springer Science & Business Media, Berlin
- Sant'Anna LG, Riccomini C, Rodrigues-Francisco BH, Sial AN, Carvalho MD, Moura CAV (2004) The Paleocene travertine system of the Itaboraí basin, Southeastern Brazil. *J South Am Earth Sci* 18(1):11–25
- Scholle P, Ulmer-Scholle D (2003) *A color guide to the petrography of carbonate rocks: grains, textures, porosity, diagenesis*. AAPG
- Seber GAF (1984) *Multivariate observations*. Wiley, New York
- Soete J, Kleipool LM, Claes H, Claes S, Hamaekers H, Kele S, Özkul M, Foubert A, Reijmer JGG, Swennen R (2015) Acoustic properties in travertines and their relation to porosity and pore types. *Mar Pet Geol* 59:320–335
- Tucker ME, Wright VP (1990) Carbonate mineralogy and chemistry. In: *Carbonate sedimentology*. Blackwell Publishing Ltd., Oxford. doi:[10.1002/9781444314175.ch6](https://doi.org/10.1002/9781444314175.ch6)
- Verwer K, Eberli G, Baechle G, Weger R (2010) Effect of carbonate pore structure on dynamic shear moduli. *Geophysics* 75(1):E1
- Warren J (2000) Dolomite: occurrence, evolution and economically important associations. *Earth Sci Rev* 52(1–3):1–81
- Wentworth CK (1923) *The shapes of beach pebbles*, US Government Printing Office
- Wightman FL, Kistler DJ (1989) Headphone simulation of free-field listening. II: Psychophysical validation. *J Acoust Soc Am* 85(2):868–878
- Wirjadi O (2007) *Survey of 3D image segmentation methods*. ITWM, Kaiserslautern
- Wright VP, Barnett AJ (2015) An abiotic model for the development of textures in some South Atlantic early Cretaceous lacustrine carbonates Cretaceous. *Geol Soc London Spec Publ* 418(2012):1–11